JCTC Journal of Chemical Theory and Computation

Article

pubs.acs.org/JCTC

The Performance of Density Functionals for Sulfate−Water Clusters

Narbe Mardirossian,[†] Daniel S. Lambrecht,[‡] Laura McCaslin,[§] Sotiris S. Xantheas,[∥] and Martin Head-Gordon[†,*]

[†]Department of Chemistry, University of California, Berkeley, California, United States

[‡]Department of Chemistry, University of Pittsburgh, Pittsburgh, Pennsylvania, United States

[§]Department of Chemistry and Biochemistry, University of Texas—Austin, Texas, United States

[∥]Physical Sciences Division, Pacific Northwest National Laboratory, Richland, Washington, United States

Supporting Information

ABSTRACT: The performance of 24 density functionals, Hartree−Fock, and MP2 is assessed with respect to the CCSD(T)/CBS* energetics of 49 sulfate−water clusters with three to six water molecules. Included among the density functionals are GGA, meta-GGA, hybrid GGA, hybrid meta-GGA, and double hybrid density functionals, as well as the LDA. Three types of dispersion corrections (VV10, XDM, and -D) are tested in conjunction with these functionals. The 26 methods are compared using the relative and binding energies of the sulfate−water clusters as the main criteria. It was discovered that a majority of the tested density functionals are unable to simultaneously capture the physics necessary to describe both the relative and binding energies of the anionic solvation clusters. The three density functionals with the best overall performance are XYG3, ωB97X-2, and XYGJ-OS. The only other density functional that performs comparably to these three double hybrids is M11. A majority of the density functionals that contain a fraction of exact exchange tend to perform well only for the relative energies, while functionals lacking exact exchange generally perform poorly with respect to both criteria. However, the meta-GGA functional, M11-L, stands out due to its superior performance for the relative energies. While dispersion correction functionals cannot replace the accuracy provided by MP2 correlation, it is shown that the proper combination of a hybrid GGA functional (LC-ωPBE) with a dispersion correction functional (VV10) can lead to drastic improvements in the binding energies of the parent functional, while preserving its performance with respect to the relative energies. Ultimately, however, MP2 has the best overall performance out of the 26 benchmarked methods.

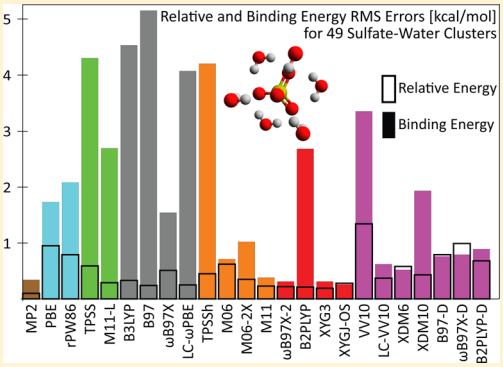

1. INTRODUCTION

Density functional theory[1,2] is the sweet spot between computational cost (typically scaling as $O(N^3)$ or better with system size) and accuracy. This has made DFT the method of choice for a majority of today's molecular calculations. However, the famous Jacob's ladder[3] of DFT does not provide as straightforward an approach to systematically reliable results as the clear-cut hierarchy of wave function-based (WF) methods. Therefore, it is *necessary* to test the accuracy of density functionals to determine the range of their applicability and identify areas for improvement.

Computational chemists of the 21st century have a wide variety of density functionals at their disposal, ranging from the well-established LDA to modern-day double hybrid density functionals. With so many functionals to choose from, picking the *best* functional for a particular application becomes a difficult task. Luckily, the computational chemistry literature contains an abundance of up-to-date density functional benchmarks[4−11] which facilitate the task of picking a functional. However, for very specific DFT applications, such as aqueous solvation clusters of anions, benchmarks that deal primarily with thermochemical data (atomization energies, barrier heights, etc.) can be too generic. Therefore, the following analysis attempts to assess the performance of a variety of density functionals by focusing on a very specific class of molecules: sulfate−water clusters, $SO_4^{2-}(H_2O)_n$.

Sulfate plays an important role in chemistry due to its ubiquitous involvement in several technical, biological, and environmental contexts.[12−14] In general, studying aqueous solvation clusters of anions provides a unique window into understanding the complicated nature of solvation.[15−17] Specifically, sulfate−water clusters allow for joint experimental and theoretical insights into nanosolvation due to the possibility of mass selecting clusters of well-defined sizes and investigating them spectroscopically.[18−20]

In a recent paper,[21] high-level electronic structure results for the relative and binding energies of 49 sulfate−water clusters, $SO_4^{2-}(H_2O)_n$ (n = 3−6), were obtained in an effort to understand the relative populations of these structures at various temperatures and correlate them with experimental data. The benchmark results are of coupled cluster singles and

Received: September 28, 2012
Published: January 30, 2013

   dx.doi.org/10.1021/ct4000235 | J. Chem. Theory Comput. 2013, 9, 1368−1380

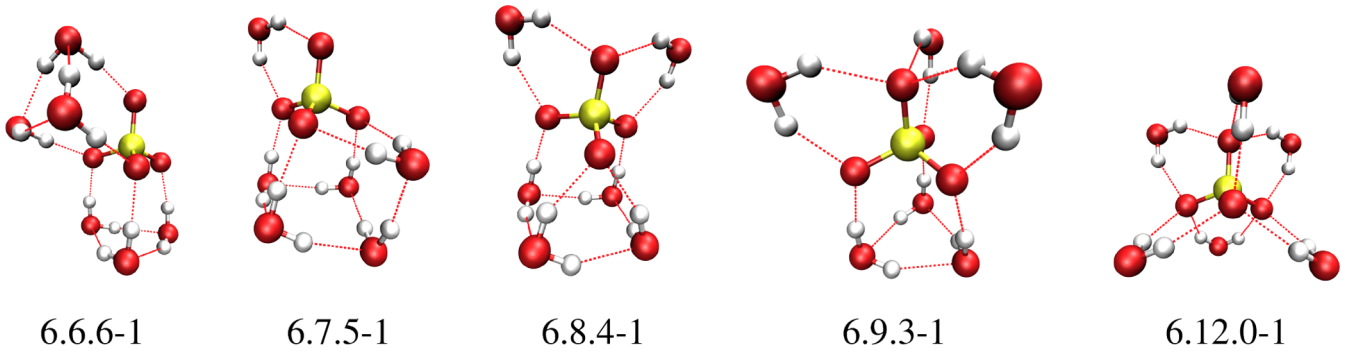

Figure 1. Gallery of representative binding motifs. One representative from each hydrogen bonding network class according to the "*n.s.w*−*l*" nomenclature is shown for $n = 6$.

doubles with perturbative triples (CCSD(T)) quality at the estimated complete basis set (CBS*) limit. These CCSD(T)/CBS* results are used to assess the performance of five distinct classes of density functionals: GGA functionals (PBE+PBE [PBE][22] and rPW86+PBE [rPW86][23]), meta-GGA functionals (TPSS[24] and M11-L[25]), hybrid GGA functionals (B3LYP,[26] B97,[27] ωB97X,[28] and ωPBE+PBE [LC-ωPBE][29]), hybrid meta-GGA functionals (TPSSh,[30] M06,[31] M06-2X,[31] and M11[32]), and double hybrid density functionals (ωB97X-2,[33] B2PLYP,[34] XYG3,[35] and XYGJ-OS[36]). In addition, several dispersion-corrected versions of these functionals are benchmarked: rPW86+PBE+VV10 [VV10],[37] ωPBE+PBE+VV10 [LC-VV10],[37] B3LYP+XDM6 [XDM6],[38−43] B3LYP+XDM10 [XDM10],[38−43] B97-D,[44] ωB97X-D,[45] and B2PLYP-D.[46] Hartree−Fock (HF), second-order Møller−Plesset perturbation theory (MP2), and LDA (SVWN) results are provided for comparison to the DFT results.

The purpose of this study is 2-fold: first, to test the potential of applying DFT to larger sizes of these clusters (which would be too costly using standard wave function-based methods) and, second, to try to understand the strengths and failures of a variety of density functionals with respect to describing solvation effects involving anions. Presently, many density functionals have well-known shortcomings such as an incomplete treatment of dispersion interactions[47−51] or qualitative failures due to self-interaction error.[52,53] While attempts have been made to remedy both of these issues (i.e., dispersion tails[44,54−59] and range-separated functionals,[28,29,32,33,45,60−72] respectively), complications still exist. For example, dispersion tails cannot differentiate between neutral, anionic, and cationic atoms, and a majority of range-separated functionals cannot properly dissociate charged diatomics like He_2^+.

2. COMPUTATIONAL DETAILS

We use our "*n.s.w*−*l*" nomenclature for the cluster isomers, as introduced in our earlier publication.[73] Within this notation, *n* represents the number of water molecules in the structure, *s* represents the number of sulfate−water bonds in the structure, *w* represents the number of water−water bonds in the structure, and *l* distinguishes each isomer from one another. In Figure 1, a selection of different binding motifs within the test set is shown for illustration.

The smallest system that was studied was $n = 3$, since clusters with $n < 3$ are unstable in the gas phase with respect to electron autodetachment,[74−76] and clusters of sizes up to $n = 6$ are included. The starting geometries were obtained from a large-scale search for low-lying structures[73] using the polarizable force field, AMOEBA.[77] From these, several sets of geometries were generated and used in subsequent calculations. All of the calculations in this paper were performed using geometries obtained via resolution-of-the-identity (RI) MP2 optimizations in the aug-cc-pVTZ basis within the dual-basis[78−84] (db) approximation (RI-MP2/db-aug-cc-pVTZ). The CCSD(T)/CBS* reference values from a previous publication[21] have been updated and are included in the Supporting Information. The updated reference data no longer employ the dual-basis approximation. For the $n = 3$−5 isomers, the relative and binding energies are calculated as follows:

$$E_{\mathrm{CCSD(T)}}^{\mathrm{CBS*}} = E_{\mathrm{HF}}^{\mathrm{aQZ}} + E_{\mathrm{RI-MP2}}^{\mathrm{a(TQ)Z}} + [E_{\mathrm{CCSD(T)}}^{\mathrm{aTZ}} - E_{\mathrm{MP2}}^{\mathrm{aTZ}}] \quad (1)$$

For the $n = 6$ isomers, the relative energies are calculated by employing the aug-cc-pVDZ basis for the ΔCC term (the term in brackets in eq 1) instead of the aug-cc-pVTZ basis. The use of a smaller basis is justified by noting that for the five $n = 6$ isomers for which we have both aug-cc-pVDZ and aug-cc-pVTZ ΔCC values, the largest difference in the relative energies between the two basis sets is 0.02 kcal/mol. Furthermore, the average binding energy difference between the two basis sets for these five $n = 6$ isomers is −0.21 kcal/mol with a standard deviation of −0.012 kcal/mol. Therefore, a correction factor of 0.21 kcal/mol is added to the remaining 13 aug-cc-pVDZ binding energies to correct them toward the aug-cc-pVTZ level. Thus, we keep the five existing $n = 6$ aug-cc-pVTZ binding energies and use the 13 corrected "aug-cc-pVTZ" binding energies instead of the original aug-cc-pVDZ ones. In eq 1, $E_{\mathrm{RI-MP2}}^{\mathrm{a(TQ)Z}}$ indicates a (TQ) extrapolation[85] of aug-cc-pVTZ and aug-cc-pVQZ RI-MP2 correlation energies. Finally, in order to ensure that the RI-MP2/aug-cc-pV(TQ)Z values are at the basis set limit, the lowest and highest energy $n = 3$ isomers were calculated in the aug-cc-pV5Z basis set. The RI-MP2/CBS aug-cc-pV(Q5)Z $n = 3$ isomer energy range is 3.55 kcal/mol, compared to the RI-MP2/CBS aug-cc-pV(TQ)-Z value of 3.50 kcal/mol. Thus, we believe the existing RI-MP2/CBS values to be of sound quality.

Calculations for all 26 benchmarked methods were performed in both the aug-cc-pVTZ and aug-cc-pVQZ basis sets. For the double hybrid density functionals (DHDFs), aug-cc-pVTZ and aug-cc-pV(TQ)Z results are presented, while for the remaining density functionals, only the aug-cc-pVQZ data are included since there is no considerable difference in the statistics between the two basis sets. The HF results that are provided for comparison to the DFT results are from the aug-

dx.doi.org/10.1021/ct4000235 | J. Chem. Theory Comput. 2013, 9, 1368−1380

cc-pVQZ calculations, while RI-MP2 results in both the aug-cc-pVTZ and aug-cc-pV(TQ)Z basis sets are included.

The main concern of this benchmark is the performance of the considered methods with respect to energetics. As a result, two different measures are used for comparison. First, the performance for relative isomer energies, E_{rel}, calculated relative to the global minimum for each cluster size (as predicted by each method) is reported.

In addition to the relative energies, we consider the binding energies, E_{bind}, defined by

$$E_{bind} = E(n.\ s.\ w - l) - E(3.6.0 - 1) - (n - 3)\cdot E(H_2O) \quad (2)$$

where $E(X)$ is the energy of isomer or molecule X. $E(3.6.0-1)$ is the energy of the 3.6.0−1 isomer and was chosen as the reference for zero energy since it is the lowest-lying stable $n = 3$ isomer according to the CCSD(T)/CBS* calculations. Counterpoise corrections are not performed, since basis set superposition errors are expected to be small due to the large basis sets used.

Besides E_{rel} and E_{bind}, a third useful measure of performance is the "aligned binding energy" ($E_{aligned}$), namely, the binding energy corrected for systematic errors. To calculate $E_{aligned}$, the mean signed error (MSE) in the binding energy for each cluster size, n, is subtracted from the binding energy: $E_{aligned} = E_{bind} -$ MSE. While $E_{aligned}$ is not directly used to assess the quality of the methods, it is used in conjunction with E_{bind} to compute the BAR, the total E_{bind} RMSD to total $E_{aligned}$ RMSD ratio. Large values for the BAR indicate that a given method is systematically underbinding or overbinding the sulfate−water clusters.

Of the 49 total sulfate−water clusters, there are 9, 10, 12, and 18 with 3, 4, 5, and 6 water molecules, respectively. Furthermore, the average binding energies for the $n = 4-6$ isomers are −21.13, −42.09, and −62.11 kcal/mol, respectively.

All of the DFT calculations were performed with a development version of Q-Chem 4.0.[86] For the density functional calculations, an integration grid of 100 radial and 302 angular points was used, which led to errors of less than a few tens of μHartrees for the more grid-sensitive functionals.[87] All of the calculations for the DHDFs and MP2 were performed within the frozen core approximation and the resolution-of-the-identity approximation. The CCSD(T) calculations were performed with the NWChem suite of codes.[88]

3. RESULTS

In total, the performance of 26 methods is compared to the CCSD(T)/CBS* reference values. In order to allow comparisons between different methods, three tables of statistics are provided. Tables 1 and 2 contain root-mean-square-deviation (RMSD) statistics for E_{rel} and E_{bind}, respectively, while Table 3 contains mean signed error (MSE) statistics for E_{bind}. The tables are horizontally divided into functional categories (WF, LDA, GGA, meta-GGA, hybrid GGA, hybrid meta-GGA, DHDF, VV10, XDM, -D) and vertically into $n = 3$, $n = 4$, $n = 5$, $n = 6$, and overall $n = 3-6$ statistics.

Furthermore, five figures will be referenced throughout the following analysis. Figure 2 plots the MSE of the binding energies for all methods (except HF and SVWN) with respect to the number of water molecules, sulfate−water bonds, and water−water bonds. Figure 3 plots the $n = 3-6$ binding energy errors for the 12 GGA, meta-GGA, hybrid GGA, and hybrid meta-GGA functionals. Figure 4 plots the $n = 3-6$ binding energy errors for the double hybrid density functionals and MP2. Figure 5 plots the $n = 3-6$ binding energy errors for the three best double hybrid density functionals (XYG3, ωB97X-2, and XYGJ-OS) and MP2 in both the aug-cc-pVTZ and aug-cc-pV(TQ)Z basis sets. Finally, Figure 6 plots the $n = 3-6$ binding energy errors for the dispersion-corrected density functionals and their nondispersion-corrected counterparts (except B2PLYP-D and B2PLYP).

Table 1. Relative Energy RMSDs (kcal/mol) with Respect to the CCSD(T)/CBS* Reference Values for All Benchmarked Methods[a]

	$n = 3$	$n = 4$	$n = 5$	$n = 6$	all
HF	1.15	2.29	2.63	2.54	2.32
MP2/aTZ	0.32	0.36	0.28	0.37	0.34
MP2/a(TQ)Z	0.07	0.11	0.08	0.11	0.10
SVWN	2.64	3.40	3.12	4.59	3.71
PBE	0.55	1.02	0.76	1.17	0.95
rPW86	0.53	0.85	0.63	0.94	0.79
TPSS	0.37	0.61	0.44	0.73	0.59
M11-L	0.21	0.32	0.29	0.31	0.29
B3LYP	0.28	0.47	0.34	0.25	0.33
B97	0.28	0.29	0.27	0.16	0.24
ωB97X	0.29	0.53	0.45	0.61	0.51
LC-ωPBE	0.22	0.24	0.29	0.24	0.25
TPSSh	0.28	0.49	0.35	0.54	0.45
M06	0.36	0.54	0.56	0.77	0.62
M06-2X	0.26	0.38	0.26	0.42	0.35
M11	0.33	0.25	0.16	0.19	0.23
ωB97X-2/aTZ	0.35	0.37	0.30	0.37	0.35
ωB97X-2/a(TQ)Z	0.20	0.24	0.19	0.24	0.22
B2PLYP/aTZ	0.24	0.35	0.21	0.25	0.26
B2PLYP/a(TQ)Z	0.17	0.29	0.21	0.17	0.21
XYG3/aTZ	0.16	0.23	0.15	0.20	0.19
XYG3/a(TQ)Z	0.08	0.13	0.11	0.11	0.11
XYGJ-OS/aTZ	0.23	0.32	0.23	0.31	0.28
XYGJ-OS/a(TQ)Z	0.10	0.20	0.15	0.18	0.16
VV10	0.67	1.33	1.17	1.65	1.34
LC-VV10	0.21	0.34	0.31	0.46	0.37
XDM6	0.39	0.64	0.44	0.70	0.58
XDM10	0.35	0.54	0.33	0.46	0.43
B97-D	0.56	0.88	0.53	0.97	0.79
ωB97X-D	0.57	1.06	0.77	1.23	0.99
B2PLYP-D/aTZ	0.51	0.85	0.59	0.93	0.77
B2PLYP-D/a(TQ)Z	0.49	0.75	0.50	0.82	0.68

[a]Results for the double hybrid density functionals and MP2 are presented in both the aug-cc-pVTZ and aug-cc-pV(TQ)Z basis sets, while the results for the remaining functionals are presented only in the aug-cc-pVQZ basis set.

These figures were created with the intention of simplifying comparisons between functionals from the same rung. GGA functionals are indicated by circular markers. meta-GGA functionals are indicated by stars. Hybrid GGA functionals are indicated by triangles. Hybrid meta-GGA functionals are indicated by musical symbols, and double hybrid density functionals are indicated by rectangles. Furthermore, in order to facilitate comparisons between a functional and its dispersion-corrected counterpart, the marker that is used for the parent functional is filled.

3.1. Performance of CDFs: Conventional Density Functionals. *3.1.1. Motivation.* As stated in the Introduction, a primary goal of this paper is to identify density functionals

Table 2. Binding Energy RMSDs (kcal/mol) with Respect to the CCSD(T)/CBS* Reference Values for All Benchmarked Methods[a]

	$n = 3$	$n = 4$	$n = 5$	$n = 6$	All
HF	1.15	6.03	11.25	15.92	11.48
MP2/aTZ	0.32	0.52	0.85	1.11	0.84
MP2/a(TQ)Z	0.07	0.16	0.32	0.47	0.34
SVWN	1.85	7.40	13.90	19.72	14.21
PBE	0.66	0.95	1.62	2.39	1.73
rPW86	0.53	1.09	1.98	2.90	2.08
TPSS	0.37	2.06	4.13	6.05	4.30
M11-L	0.21	1.18	2.53	3.84	2.69
B3LYP	0.28	2.31	4.40	6.33	4.53
B97	0.28	2.53	4.97	7.21	5.15
ωB97X	0.29	0.79	1.51	2.13	1.54
LC-ωPBE	0.22	2.00	3.93	5.72	4.07
TPSSh	0.28	2.04	4.04	5.89	4.20
M06	0.36	0.59	0.82	0.81	0.71
M06-2X	0.26	0.62	1.10	1.34	1.02
M11	0.33	0.20	0.30	0.51	0.38
ωB97X-2/aTZ	0.35	0.50	0.82	1.11	0.83
ωB97X-2/a(TQ)Z	0.20	0.22	0.30	0.40	0.31
B2PLYP/aTZ	0.24	1.18	2.23	3.21	2.30
B2PLYP/a(TQ)Z	0.17	1.38	2.61	3.73	2.68
XYG3/aTZ	0.16	0.23	0.31	0.40	0.31
XYG3/a(TQ)Z	0.08	0.48	0.84	1.13	0.83
XYGJ-OS/aTZ	0.23	0.23	0.25	0.29	0.26
XYGJ-OS/a(TQ)Z	0.10	0.33	0.58	0.78	0.57
VV10	0.90	1.94	3.34	4.54	3.35
LC-VV10	0.21	0.42	0.66	0.80	0.62
XDM6	0.39	0.41	0.49	0.65	0.52
XDM10	0.35	1.06	1.87	2.67	1.93
B97-D	0.72	0.58	0.65	0.91	0.76
ωB97X-D	0.81	0.79	0.84	0.75	0.79
B2PLYP-D/aTZ	0.60	0.81	1.28	1.65	1.27
B2PLYP-D/a(TQ)Z	0.49	0.60	0.91	1.14	0.89

[a]Results for the double hybrid density functionals and MP2 are presented in both the aug-cc-pVTZ and aug-cc-pV(TQ)Z basis sets, while the results for the remaining functionals are presented only in the aug-cc-pVQZ basis set.

Table 3. Binding Energy MSEs (kcal/mol) with Respect to the CCSD(T)/CBS* Reference Values for All Benchmarked Methods[a]

	$n = 3$	$n = 4$	$n = 5$	$n = 6$	all
HF	0.81	5.85	11.12	15.81	9.87
MP2/aTZ	−0.24	−0.43	−0.81	−1.08	−0.73
MP2/a(TQ)Z	−0.05	0.14	0.31	0.46	0.27
SVWN	−1.18	−6.99	−13.59	−19.43	−12.11
PBE	−0.43	0.66	1.43	2.20	1.21
rPW86	−0.34	0.93	1.88	2.80	1.62
TPSS	−0.20	2.02	4.11	6.02	3.59
M11-L	−0.08	1.15	2.52	3.83	2.24
B3LYP	−0.03	2.29	4.39	6.32	3.86
B97	−0.08	2.52	4.97	7.21	4.36
ωB97X	−0.18	−0.69	−1.44	−2.07	−1.29
LC-ωPBE	0.13	1.99	3.92	5.71	3.49
TPSSh	−0.11	2.01	4.03	5.87	3.53
M06	−0.21	−0.39	−0.63	−0.62	−0.50
M06-2X	−0.16	−0.56	−1.08	−1.32	−0.89
M11	0.22	0.12	0.26	0.48	0.30
ωB97X-2/aTZ	−0.26	−0.41	−0.77	−1.07	−0.71
ωB97X-2/a(TQ)Z	−0.14	−0.13	−0.24	−0.34	−0.23
B2PLYP/aTZ	−0.11	1.16	2.22	3.20	1.94
B2PLYP/a(TQ)Z	−0.02	1.36	2.61	3.73	2.28
XYG3/aTZ	−0.09	0.17	0.27	0.35	0.21
XYG3/a(TQ)Z	0.03	0.47	0.84	1.12	0.72
XYGJ-OS/aTZ	−0.15	−0.04	−0.10	−0.14	−0.11
XYGJ-OS/a(TQ)Z	−0.02	0.31	0.56	0.76	0.48
VV10	−0.64	−1.66	−3.14	−4.36	−2.83
LC-VV10	−0.13	−0.34	−0.58	−0.72	−0.50
XDM6	−0.25	0.09	0.21	0.38	0.17
XDM10	−0.18	1.00	1.84	2.65	1.60
B97-D	−0.51	0.18	0.38	0.74	0.31
ωB97X-D	−0.57	−0.23	−0.41	−0.23	−0.33
B2PLYP-D/aTZ	−0.42	−0.56	−1.14	−1.54	−1.04
B2PLYP-D/a(TQ)Z	−0.33	−0.36	−0.76	−1.01	−0.69

[a]Results for the double hybrid density functionals and MP2 are presented in both the aug-cc-pVTZ and aug-cc-pV(TQ)Z basis sets, while the results for the remaining functionals are presented only in the aug-cc-pVQZ basis set.

that can be applied to larger sulfate−water clusters ($n \geq 7$). In the aug-cc-pVTZ basis set, a single-point calculation on each of the $n = 6$ isomers involves 786 basis functions, with each additional water molecule contributing 92 basis functions, while in the aug-cc-pVQZ basis set, the number of basis functions is 1436 and 172, respectively. Therefore, due to the large number of basis functions involved in calculations on large clusters, the ideal scenario is to identify the least expensive DFT method that performs satisfactorily for the energetics of the $n = 3$−6 clusters. As a result, the natural starting point is GGA functionals. Closely related to GGA functionals are meta-GGA functionals that take into account both the first and second derivative of the density (or the kinetic energy density). Finally, since the inclusion of a fraction of exact exchange has been shown to dramatically improve the results of gradient-based functionals,[26] hybrid density functionals have the potential of performing well for the present system. Thus, this section evaluates the performance of two GGA functionals (PBE[22] and rPW86[23]), two meta-GGA functionals (TPSS[24] and M11-L[25]), four hybrid GGA functionals (B3LYP,[26] B97,[27] ωB97X,[28] and LC-ωPBE[29]), and four hybrid meta-GGA functionals (TPSSh,[30] M06,[31] M06-2X,[31] and M11[32]) for the energetics of the sulfate−water clusters.

The functionals in this section will be referred to as conventional density functionals (CDFs). The percentage of exact exchange included in B3LYP and B97 is 20% and 19%, respectively, while the latter two hybrid GGA functionals are range-separated hybrid (RSH) functionals. For ωB97X, the percentage of exact exchange starts at 16% and increases to 100% ($\omega = 0.3$), while for LC-ωPBE, the percentage of exact exchange starts at 0% and increases more sharply to 100% ($\omega = 0.45$). From the hybrid meta-GGA functionals, TPSSh, M06, and M06-2X have 10%, 27%, and 54% exact exchange, respectively, while M11 is an RSH with 43% short-range exact exchange and 100% long-range exact exchange ($\omega = 0.25$).

3.1.2. E_{rel}: CDFs. From the 12 density functionals considered in this section, the four functionals with the best overall performance for the relative energies are M11, B97, LC-ωPBE, and M11-L, with total RMSDs of 0.23, 0.24, 0.25, and 0.29 kcal/mol, respectively. In comparison, HF, MP2, and SVWN have total RMSDs of 2.32, 0.10, and 3.71 kcal/mol,

dx.doi.org/10.1021/ct4000235 | J. Chem. Theory Comput. 2013, 9, 1368−1380

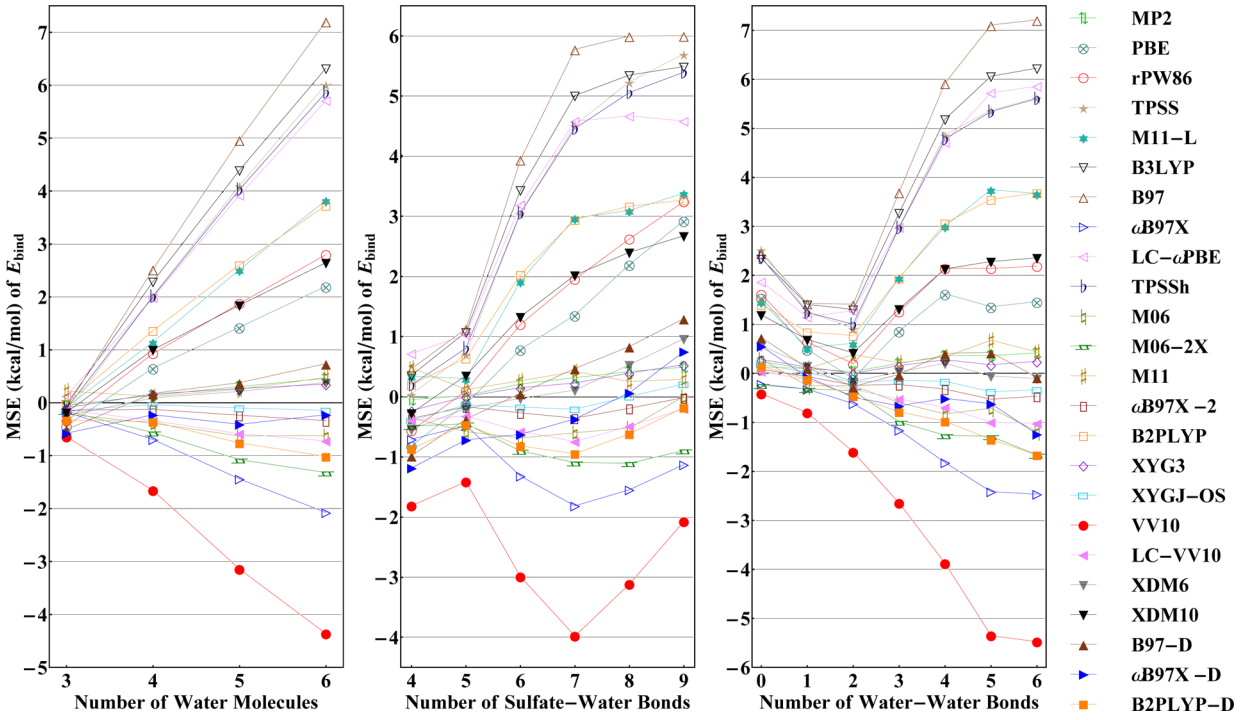

Figure 2. Mean signed error (MSE) of the binding energies for all methods (except HF and SVWN) with respect to the number of water molecules, sulfate−water bonds, and water−water bonds. Results for the double hybrid density functionals are presented in the basis that most closely resembles the basis in which the respective functionals were parametrized (aug-cc-pV(TQ)Z for ωB97X-2, B2PLYP, and B2PLYP-D and aug-cc-pVTZ for XYG3 and XYGJ-OS). The MP2 results are from aug-cc-pV(TQ)Z calculations, while the results for the remaining functionals are presented in the aug-cc-pVQZ basis set. GGA functionals are indicated by circular markers. meta-GGA functionals are indicated by stars. Hybrid GGA functionals are indicated by triangles. Hybrid meta-GGA functionals are indicated by musical symbols, and double hybrid density functionals are indicated by rectangles. Furthermore, in order to facilitate comparisons between a functional and its dispersion-corrected counterpart, the marker that is used for the parent functional is filled. The errors are with respect to the CCSD(T)/CBS* reference values described in section 2.

respectively, with MP2 affording the smallest total E_{rel} RMSD of all the methods considered and SVWN, the largest.

The dramatic 4-fold improvement that results from replacing the PBE exchange functional in PBE with the long-range-corrected hybrid ωPBE exchange functional in LC-ωPBE attests to the significant role that exact exchange plays in computing relative energies. The same phenomenon is apparent when comparing M06 and M06-2X (doubling the amount of exact exchange almost halves the overall relative energy RMSD) as well as TPSS and TPSSh (including exact exchange improves the total E_{rel} RMSD by 0.14 kcal/mol). Furthermore, the two GGA functionals exhibit the worst performance for the relative energies, again confirming that exact exchange is necessary for properly describing the relative energetics of these clusters. On a related note, PBE predicts the incorrect n = 3 global minimum (3.3.3−1 instead of 3.6.0−1), while for the larger clusters (n = 4−6), all 12 functionals predict the correct lowest-energy isomers of 4.5.3−1, 5.7.3−1, and 6.6.6−1. Comparing the performance of the GGA functionals to the meta-GGA functionals, it is clear that dependence on the kinetic energy density is advantageous for the relative energies of these clusters, as both TPSS and M11-L perform better than PBE and rPW86. However, there is no clear hierarchy when comparing the hybrid GGA and hybrid meta-GGA functionals.

It is shocking that B97 performs more than 2 times better than its more advanced counterpart, ωB97X. While it is difficult to pinpoint the exact cause of this behavior, it is meaningful to consider the major differences between the forms of the two functionals. B97 and ωB97X have three major differences: (1) B97 has a fixed amount of exact exchange (19%), while ωB97X features range-separation with the percentage of exact exchange increasing from 16% at short-range to 100% at long-range. (2) The power series expansion of the exchange, opposite-spin correlation, and same-spin correlation inhomogeneity correction factors was truncated at m = 2 for B97, while for ωB97X, it was truncated at m = 4. (3) The uniform electron gas (UEG) limit for exchange and correlation *was not* imposed for B97, while it *was* imposed for ωB97X. Thus, while the optimization of B97 inadvertently recovered the UEG limit for exchange and opposite-spin correlation, it did not recover the UEG limit for same-spin correlation, optimizing the leading term to 0.17 instead of 1.0 (as in ωB97X). Since it was determined earlier that having exact exchange is advantageous for the relative energies (and since two of the four best functionals are range-separated hybrid functionals), the poor performance of ωB97X for the relative energies compared to B97 is likely due to either its greater number of empirical parameters or its UEG constraint on same-spin correlation. In order to pinpoint the reason, aug-cc-pVTZ calculations were performed with the BLYP and BPW91 functionals, since the only difference between the two is that the PW91 correlation functional imposes the UEG constraint while the LYP correlation functional does not. The total E_{rel} RMSD for both functionals was identically 0.43 kcal/mol, hinting that the UEG constraint on correlation does not play a major role in predicting the correct energetic ordering for the present system. Thus, it can be concluded that the poor performance of ωB97X compared to B97 is a byproduct of its m = 4 power series expansion which causes the functional to be less transferable when considering systems outside of its training set.

dx.doi.org/10.1021/ct4000235 | J. Chem. Theory Comput. 2013, 9, 1368−1380

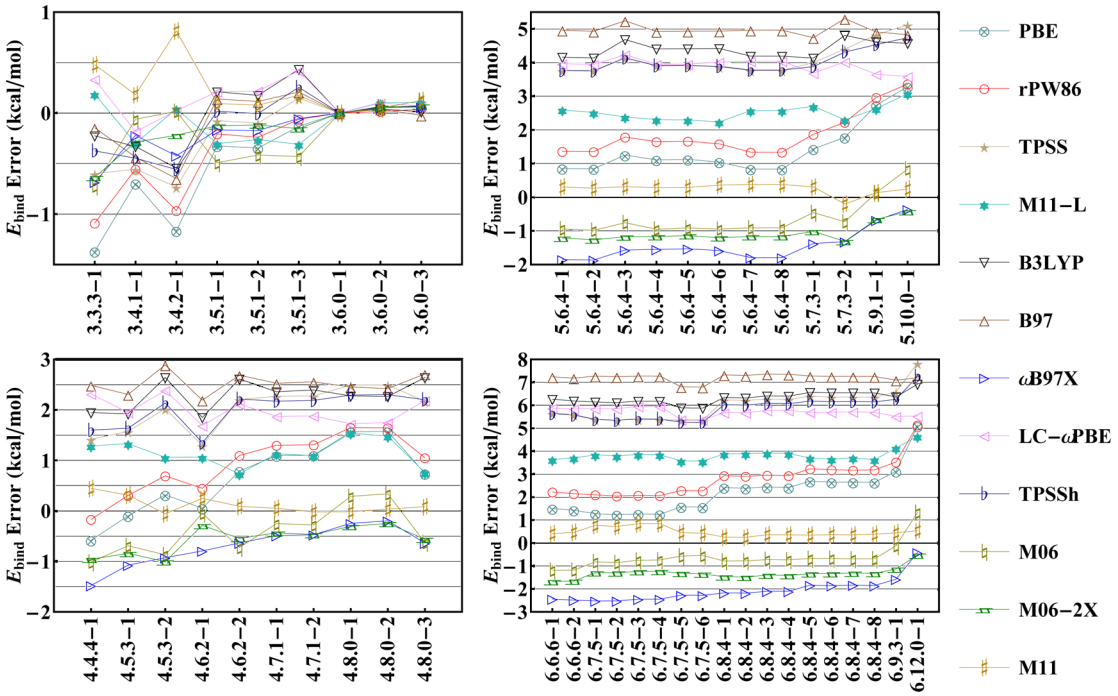

Figure 3. n = 3−6 binding energy errors for the 12 GGA, meta-GGA, hybrid GGA, and hybrid meta-GGA functionals. All of the results are from calculations in the aug-cc-pVQZ basis set. GGA functionals are indicated by circular markers. meta-GGA functionals are indicated by stars. Hybrid GGA functionals are indicated by triangles, and hybrid meta-GGA functionals are indicated by musical symbols. The errors are with respect to the CCSD(T)/CBS* reference values described in section 2. The cluster isomers are labeled using the "*n.s.w*−*l*" nomenclature described in section 2, where n represents the number of water molecules in the structure, s represents the number of sulfate−water bonds in the structure, w represents the number of water−water bonds in the structure, and l distinguishes each isomer from one another.

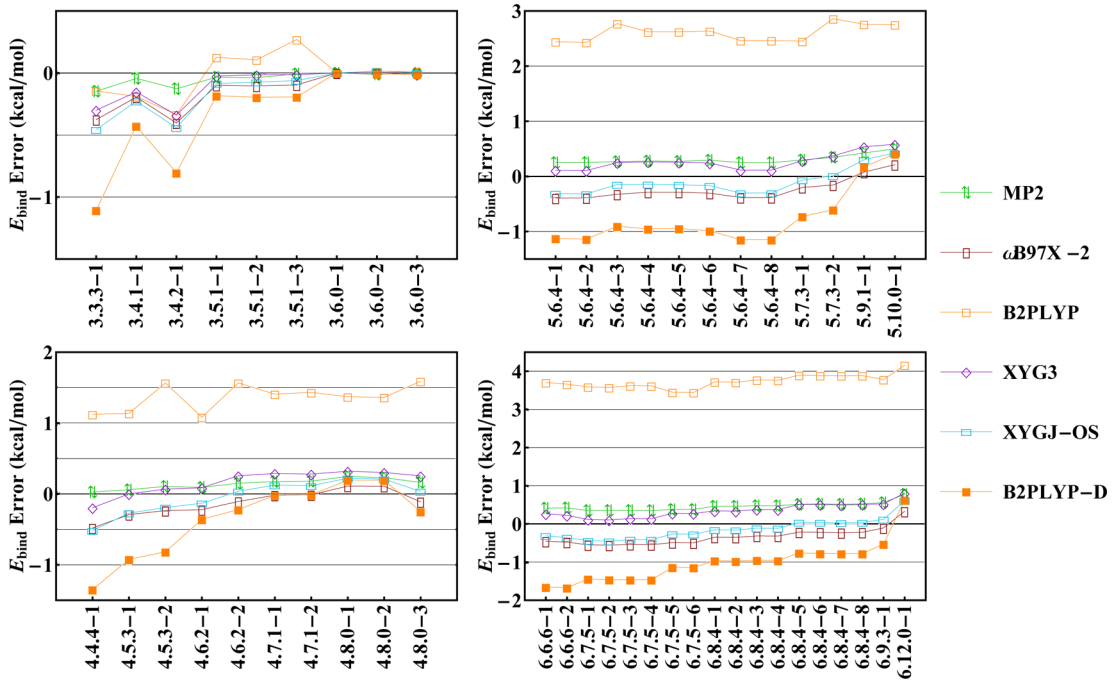

Figure 4. n = 3−6 binding energy errors for the double hybrid density functionals and MP2. Results for the double hybrid density functionals are presented in the basis that most closely resembles the basis in which the respective functionals were parametrized (aug-cc-pV(TQ)Z for ωB97X-2, B2PLYP, and B2PLYP-D and aug-cc-pVTZ for XYG3 and XYGJ-OS). The MP2 results are from aug-cc-pV(TQ)Z calculations. The errors are with respect to the CCSD(T)/CBS* reference values described in section 2. The cluster isomers are labeled using the "*n.s.w*−*l*" nomenclature described in section 2, where n represents the number of water molecules in the structure, s represents the number of sulfate−water bonds in the structure, w represents the number of water−water bonds in the structure, and l distinguishes each isomer from one another.

The remarkable performance of M11-L for the relative energies is definitely noteworthy. Unlike conventional range-separated hybrid DFT functionals that partition the exchange energy into a short-range DFT component and a long-range

dx.doi.org/10.1021/ct4000235 | J. Chem. Theory Comput. 2013, 9, 1368−1380

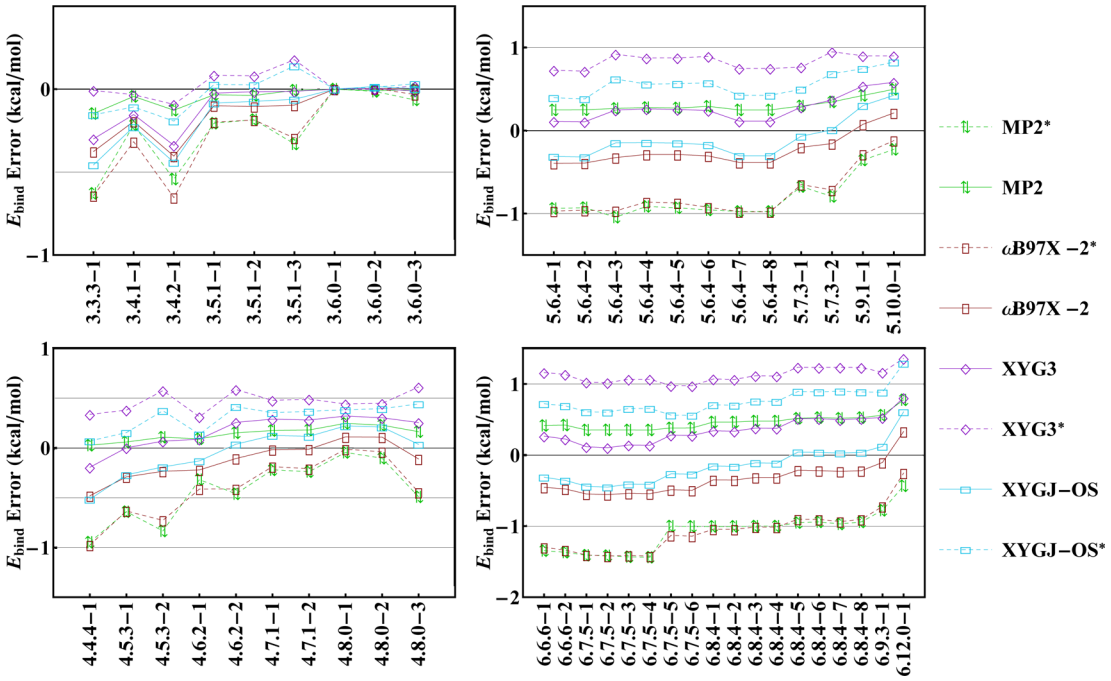

Figure 5. n = 3−6 binding energy errors for the three best double hybrid density functionals (XYG3, ωB97X-2, and XYGJ-OS) and MP2 in both the aug-cc-pVTZ and aug-cc-pV(TQ)Z basis sets. Solid lines represent results from the basis that most closely resembles the basis in which the respective functionals were parametrized (aug-cc-pV(TQ)Z for ωB97X-2 and aug-cc-pVTZ for XYG3 and XYGJ-OS). Dashed lines (accompanied by asterisks in the legend) represent results from the alternative, nonstandard basis set. The solid line for MP2 consists of aug-cc-pV(TQ)Z values, while the dashed line consists of aug-cc-pVTZ values. The errors are with respect to the CCSD(T)/CBS* reference values described in section 2. The cluster isomers are labeled using the "*n.s.w*−*l*" nomenclature described in section 2, where *n* represents the number of water molecules in the structure, *s* represents the number of sulfate−water bonds in the structure, *w* represents the number of water−water bonds in the structure, and *l* distinguishes each isomer from one another.

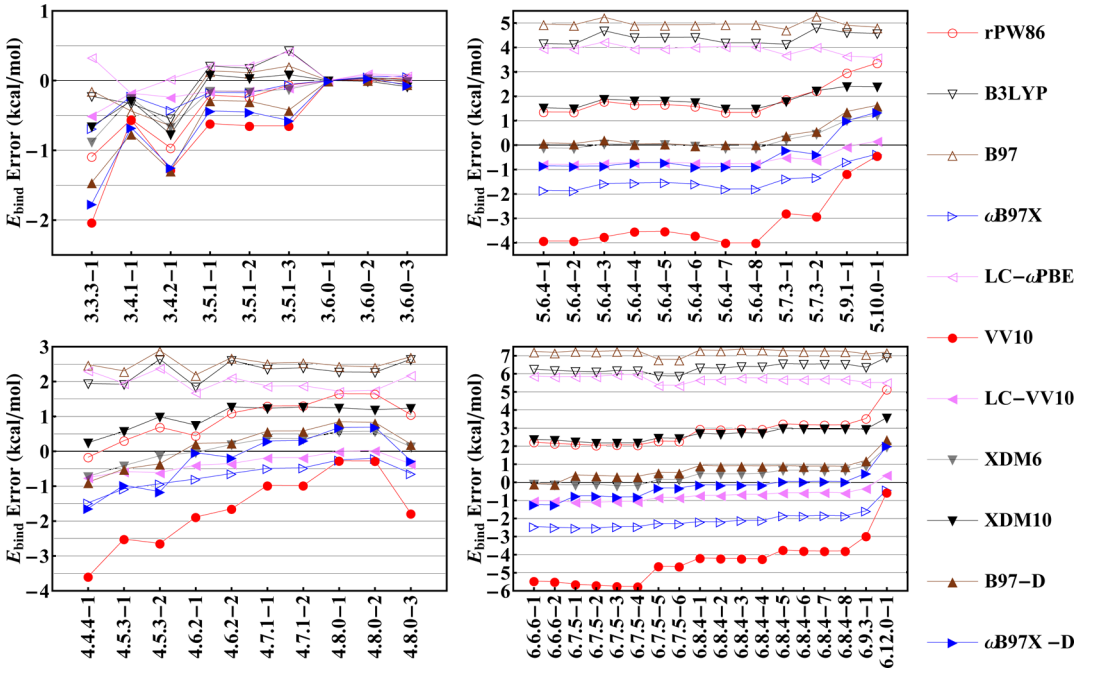

Figure 6. n = 3−6 binding energy errors for the dispersion-corrected density functionals and their nondispersion-corrected counterparts (except B2PLYP-D and B2PLYP). All of the results are from calculations in the aug-cc-pVQZ basis set. In order to facilitate comparisons between a functional and its dispersion-corrected counterpart, the marker that is used for the parent functional is filled. The errors are with respect to the CCSD(T)/CBS* reference values described in section 2. The cluster isomers are labeled using the ""*n.s.w*−*l*" nomenclature described in section 2, where *n* represents the number of water molecules in the structure, *s* represents the number of sulfate−water bonds in the structure, *w* represents the number of water−water bonds in the structure, and *l* distinguishes each isomer from one another.

dx.doi.org/10.1021/ct4000235 | J. Chem. Theory Comput. 2013, 9, 1368−1380

exact exchange component (with the erfc and erf operators, respectively), M11-L is a range-separated meta-GGA functional that partitions the exchange energy into a short-range DFT component and a long-range DFT component, both with different sets of empirical parameters for the inhomogeneity correction factors. With this functional form, M11-L attempts to mimic the nonlocal exact exchange necessary at long-range, with DFT exchange. It is clear, as far as the relative energies are concerned, that M11-L achieves this goal, as it performs comparably to M11, a hybrid functional that employs range-separation. Furthermore, while it was already established in this section that exact exchange is vital for the relative energies of these isomers, M11-L is the only functional that is able to perform well for the relative energies without explicitly including a nonlocal exchange term, further suggesting that the dual-range DFT exchange partitioning is effective.

3.1.3. E_{bind}: CDFs. From the 12 density functionals considered in this section, the two functionals with the best overall performance for the binding energies are M11 and M06, with total RMSDs of 0.38 and 0.71 kcal/mol, respectively. In comparison, HF, MP2, and SVWN have total RMSDs of 11.48, 0.34, and 14.21 kcal/mol, respectively.

While exact exchange was demonstrated to be significant for the relative energies in the previous section, the statistics in Table 2 paint a different picture for the binding energies, as the two GGA functionals perform considerably better than three of the four hybrid GGA functionals (B3LYP, B97, and LC-ωPBE). In some cases, the data suggest that exact exchange is a disadvantage for the binding energies, as the performance of M06 worsens by a factor of 1.5 when the percentage of exact exchange is doubled. Similarly, LC-ωPBE performs worse than PBE by more than a factor of 2. However, the opposite trend is seen when comparing M11 and M11-L, as the hybrid range-separation of M11 gives it a total RMSD 7 times smaller than M11-L.

The five functionals in this section with the poorest performance are B97, B3LYP, TPSS, TPSSh, and LC-ωPBE, with total binding energy RMSDs over 4 kcal/mol. Since meta-GGA, hybrid GGA, and hybrid meta-GGA functionals are included in this set of five, it is difficult to find a feature common to all five functionals that can account for their large RMSDs.

Comparing the performance of the GGA functionals to the meta-GGA functionals indicates that the GGA functionals considered perform uniformly better than the meta-GGA functionals for the binding energies. However, comparing the performance of the hybrid GGA functionals to the hybrid meta-GGA functionals indicates that the hybrid meta-GGA functionals (with the exception of TPSSh) perform uniformly better than the hybrid GGA functionals. Therefore, it is still difficult to justify the poor performance of the five functionals in question. However, a closer look at the results suggests that the quality of the binding energies may be sensitive to the degree of inhomogeneity captured by the exchange and correlation inhomogeneity correction factors in the density functionals. For example, the four functionals with the best performance in this section are M11, M06, M06-2X, and ωB97X, and the power series of the enhancement factors for all of these functionals is expanded to at least $m = 4$. For M11, the functional with the best performance, the expansion is truncated at $m = 10$ for both exchange and correlation, while for M06 and M06-2X, the expansion is truncated at $m = 11$ for exchange and $m = 4$ for correlation. On the contrary, the enhancement factors for the five functionals that perform poorly have a value for m that is less than or equal to two.

With the help of Figure 3, it is straightforward to identify the functionals that underbind or overbind the isomers. In addition, Figure 2 helps identify the cause of the underbinding or overbinding. Of the 12 functionals considered in this section, five of them drastically underbind the isomers (B97, B3LYP, TPSS, TPSSh, and LC-ωPBE), three of them moderately underbind the isomers (M11-L, rPW86, PBE), one of them slightly underbinds the isomers (M11), one of them slightly overbinds the isomers (M06), and two of them moderately overbind the isomers (ωB97X and M06-2X). For the functionals that either drastically or moderately underbind the isomers, the degree of underbinding worsens with the number of water molecules and sulfate−water bonds. However, for the functionals that moderately overbind the isomers, the degree of overbinding worsens with respect to the number of water molecules and water−water bonds. The two functionals that either slightly underbind (M11) or slightly overbind (M06) show no distinct trends.

While the performance of the GGA functionals in this section is decent considering their relative simplicity, it is readily visible from Figure 3 that the binding energies of PBE and rPW86 are highly *unsystematic* (i.e., they contain "non-parallelity errors"), while the binding energy errors of functionals like B97 are highly *systematic*. A simple way to determine whether a functional is systematically underbinding or overbinding the sulfate−water clusters is to consider the ratio of the total binding energy RMSD to the total aligned binding energy RMSD (BAR). The BAR for three of the 12 functionals considered in this section is larger than 15. Specifically, B97, LC-ωPBE, and B3LYP have BARs of 27.38, 21.64, and 17.64, confirming that these functionals systematically underbind the isomers.

It is informative to consider the performance of HF and the LDA along with this class of functionals in order to quantify the improvement that these conventional density functionals offer over their historic counterparts. As expected, the data in Table 3 indicate that HF underbinds (9.87 kcal/mol) the sulfate−water clusters almost as much as the LDA overbinds them (−12.11 kcal/mol). It is encouraging that the best CDF, M11, has a total E_{bind} MSE that is more than 30 times smaller than that of HF and the LDA.

Ultimately, the results from this section indicate that hybrid functionals, like B97, LC-ωPBE, and B3LYP, perform well in the E_{rel} category due to the inclusion of exact exchange but succumb to severe systematic errors in the binding energies due to their inability to capture the inhomogeneities that can be accounted for by functionals like M11. Therefore in section 3.3, dispersion-corrected versions of B97, LC-ωPBE, and B3LYP will be considered in order to determine if the addition of a dispersion correction functional can correct the systematic errors in the binding energies while preserving the performance of the parent functional for the relative energies.

3.2. Performance of DHDFs: Double Hybrid Density Functionals. *3.2.1. Motivation.* Due to the encouraging performance of MP2 for the energetics of the sulfate−water clusters, four DHDFs were tested in order to assess whether the addition of a fraction of the MP2 correlation energy improves the results of the first, second, third, and fourth rung density functionals discussed in section 3.1. The DHDFs that were benchmarked were ωB97X-2,[33] B2PLYP,[34] XYG3,[35] and XYGJ-OS.[36] The same-spin and opposite-spin contributions are scaled

equally in the middle two functionals (0.27 and 0.32, respectively), while in the first functional, the same-spin component is scaled by 0.53 and the opposite-spin component is scaled by 0.45. XYGJ-OS includes only the opposite-spin component of the MP2 energy, with a coefficient of 0.44. For the four DHDFs (ωB97X-2, B2PLYP, XYG3, and XYGJ-OS), the percentage of exact exchange is 64−100% (ω = 0.3), 53%, 80%, and 77%, respectively. For ωB97X-2, the ωB97X-2(TQZ) implementation is used. While both aug-cc-pVTZ and aug-cc-pV(TQ)Z results are presented for the DHDFs and MP2 in Tables 1−3 and Figure 5, it is vital that these methods are employed in the way which is most consistent with how they were parametrized. Therefore, throughout the text and in tables and figures where only one basis set result is shown, aug-cc-pV(TQ)Z data are consistently used for ωB97X-2, B2PLYP, B2PLYP-D, and MP2, while aug-cc-pVTZ data are consistently used for XYG3 and XYGJ-OS.

3.2.2. E_{rel}: DHDFs. Table 1 contains the statistics for the performance of the DHDFs for the relative energies of the sulfate−water clusters. Among the DHDFs, XYG3 has the lowest overall E_{rel} RMSD of 0.19 kcal/mol, with B2PLYP, ωB97X-2, and XYGJ-OS following closely behind with RMSDs of 0.21, 0.22, and 0.28 kcal/mol, respectively. While all four of the DHDFs predict the correct global minimum for each cluster size, it is disheartening that none of the DHDFs improve upon MP2 (total RMSD of 0.10 kcal/mol).

It is interesting to compare the E_{rel} performance of the DHDFs in the two different basis sets, as the performance of the DHDFs for the relative energies universally improves as the size of the basis set increases. The total E_{rel} RMSD of ωB97X-2 improves by 0.13 kcal/mol when going from the aug-cc-pVTZ basis to the aug-cc-pV(TQ)Z basis and by 0.12 kcal/mol for XYGJ-OS. For B2PLYP and XYG3, the total E_{rel} RMSD decreases by only 0.05 and 0.08 kcal/mol, respectively. As expected, the magnitudes of these changes are proportional to the percentage of MP2 correlation included in the functional. The largest improvement is seen for MP2, as the (TQ) extrapolation improves upon the aug-cc-pVTZ results by 0.24 kcal/mol.

In comparison to the functionals from section 3.1, all of the DHDFs except XYGJ-OS perform better than all of the CDFs, while M11, B97, and LC-ωPBE only slightly outperform XYGJ-OS. While the results of this section seem to indicate that using the (TQ) extrapolated results is universally better for the DHDFs, the data from section 3.2.3 will stress the importance of using a basis set consistent with the parametrization of the functional.

3.2.3. E_{bind}: DHDFs. The binding energy errors for the DHDFs are reported in Table 2 and summarized graphically in Figures 2, 4, and 5. XYGJ-OS performs superbly, outperforming MP2 in the total RMSD by 0.08 kcal/mol. Both XYG3 and ωB97X-2 have total E_{bind} RMSDs of 0.31 kcal/mol, which is only slightly better than MP2 (by 0.03 kcal/mol). According to Figure 2, the quality of the binding energies of XYGJ-OS does not degrade as the number of water molecules increases. The total MSE (Table 3) of XYGJ-OS is only −0.11 kcal/mol (compared to MP2 at 0.27 kcal/mol), and the RMSD basically stays constant going from n = 3 to n = 6, the defining feature which gives XYGJ-OS the edge over MP2 with respect to the overall binding energy RMSD. Being the only functional in Figure 2 with a horizontal line about the x axis (with respect to the number of water molecules) qualifies XYGJ-OS as a candidate for performing calculations on larger clusters, since it would be expected that going from n = 6 to n = 7 and higher would induce negligible error. Figure 4 clearly indicates that MP2 slightly, yet systematically, underbinds the isomers, while XYGJ-OS underbinds almost as often as it overbinds.

Compared to the rest of the DHDFs, B2PLYP performs very poorly, with an overall RMSD at least 8 times larger than the rest of the DHDFs. While XYG3 performs only slightly worse than its close relative, XYGJ-OS, it performs very similarly to MP2, and in Figure 4, their lines are usually overlapping. Consequently, XYG3 also slightly underbinds the isomers. B2PLYP is the only DHDF that drastically and systematically underbinds the isomers, and its degree of underbinding is directly correlated with the number of water molecules and sulfate−water bonds (Figure 2). The performance of B2PLYP for the binding energies resembles that of B3LYP, and while the underbinding by B2PLYP is less severe, the B2PLYP and B3LYP lines in Figures 3 and 4 are very similar in form. Contrary to B2PLYP, ωB97X-2 slightly overbinds the isomers, and it is clear (from Figures 2 and 4) that the overbinding worsens with the number of water molecules and water−water bonds.

While in section 3.2.2 it was clear that the DHDFs performed best in the (TQ) extrapolated limit, Table 2 shows that the majority of the DHDFs perform best when evaluated in a basis similar to the basis they were trained in. For example, the performance of ωB97X-2 improves by a factor of more than 2.5 when going from the aug-cc-pVTZ basis set to the aug-cc-pV(TQ)Z basis set. On the contrary, the performance of XYG3, which was trained in the 6-311+G(3df,2p) basis, worsens by more than a factor of 2.5, and the performance of XYGJ-OS, which was trained in the G3Large basis set, worsens by a factor of 2.

Compared to functionals from the lower rungs, B2PLYP performs worse than all of the hybrid meta-GGA functionals (except TPSSh). The functional unfortunately maintains the severe underbinding of B3LYP, and the addition of the perturbation correction is only able to lessen the underbinding but not correct it. It is generally expected that density functionals that incorporate a fraction of the MP2 correlation energy should perform better than or equal to MP2, and the binding energy results for three of the four DHDFs meet this expectation.

3.3. Performance of DCFs: Dispersion-Corrected Functionals. *3.3.1. Motivation.* In order to determine whether the addition of a dispersion correction functional would improve the poor E_{bind} performance of several of the functionals considered thus far, three distinct methods for accounting for dispersion and nonlocal correlation were tested: VV10,[37] XDM,[38−43] and -D.[44−46] VV10 was coupled with rPW86 [VV10] and LC-ωPBE [LC-VV10], while two variants of XDM (XDM6 and XDM10) were coupled with B3LYP. Finally, the DFT-D2 dispersion tail introduced by Grimme was used with B97 and B2PLYP, while the completely retrained dispersion-corrected functional, ωB97X-D, was tested as well. For VV10, the recommended parameters of b = 5.9 and C = 0.0093 were used, while for LC-VV10, b = 6.3, C = 0.0089, and ω = 0.45 were used. The recommended value of κ = 800 was used for XDM6, and the recommended values of a_1 = 83 and a_2 = 155 were used for XDM10. For B97-D and B2PLYP-D, s_6 coefficients of 0.75[6] and 0.55[46] were used, respectively. For all of the functionals except ωB97X-D, the parameters of the dispersion correction were trained onto the existing functional, while for ωB97X-D, the entire functional (ω and the GGA

dx.doi.org/10.1021/ct4000235 | J. Chem. Theory Comput. 2013, 9, 1368−1380

coefficients) was reparametrized along with the dispersion tail parameter. Furthermore, while B97-D and B2PLYP-D use the DFT-D2 dispersion tail, ωB97X-D uses a slightly modified dispersion tail known as the Chai−Head-Gordon (CHG) dispersion tail. In summary, the seven dispersion-corrected functionals (DCFs) that are compared in the following sections are VV10, LC-VV10, XDM6, XDM10, B97-D, ωB97X-D, and B2PLYP-D.

3.3.2. E_{rel}: DCFs. Table 1 contains the statistics for the performance of the DCFs for the relative energies of the sulfate−water clusters. The surprisingly poor performance of VV10 immediately stands out, with a total RMSD of 1.34 kcal/mol. Comparing VV10 with its parent functional, it is evident that the addition of the nonlocal correlation (NLC) functional has worsened the overall performance of rPW86 by more than 0.5 kcal/mol. However, when considering the VV10 NLC functional, it is important to keep in mind that it is solely a functional of the electron density and that the input density from the unhybridized rPW86 functional is likely the culprit for the poor performance of VV10. Consequently, the performance of LC-VV10 for the relative energies improves upon VV10 by almost 1 kcal/mol, and it is clear that this improvement is primarily due to the inclusion of exact exchange in the ωPBE exchange functional. Unfortunately, considering the parent of LC-VV10 indicates that the RSH performs almost 2 times better without the nonlocal correlation correction. In fact, the same trend can be seen for all of the dispersion-corrected functionals. The first column of Table 5 contains the factor by which the addition of the dispersion correction worsens the overall E_{rel} RMSD of the parent functional. These factors range from 1.29 for XDM10 to 3.24 for B2PLYP-D and B97-D.

The clear message is that dispersion interaction corrections, regardless of whether they are simple dispersion tails, nonlocal correlation functionals, or components based on the instantaneous dipole moment of the exchange hole, worsen the performance of their parent functionals for the energetic ordering of the present system. Although it is difficult to conclude if this result is a failure of the physics captured by the functionals or a byproduct of training on data sets that are biased toward binding energies, it is true that the dispersion-sensitive systems that are commonly found in training sets (such as the S22 data set) contain only binding energies, not relative energies. As a result, it is expected that these dispersion-corrected functionals will perform better than their non-dispersion-corrected counterparts when their performance for binding energies is evaluated in section 3.3.3.

From the seven DCFs considered, three of them (VV10, B97-D, and ωB97X-D) predict the incorrect n = 3 global minimum (3.3.3−1 instead of 3.6.0.1). For all three, this result is purely a consequence of adding the dispersion correction, as their parent functionals are able to predict the correct n = 3 global minimum. Furthermore, VV10 predicts the incorrect n = 5 global minimum (5.6.4−2 instead of 5.7.3−1), but either the removal of the VV10 NLC functional (rPW86) or the inclusion of exact exchange (LC-VV10) fixes this issue. While these results reiterate the fact that exact exchange is vital for properly predicting the energetic ordering of the present system, the strongest message imparted from this section is the undeniable fact that all of the dispersion corrections tested are unable to improve the performance of their parent functional with respect to the relative energies.

3.3.3. E_{bind}: DCFs. Since this section compares dispersion-corrected functionals to their nondispersion-corrected counterparts (nDCFs), it should be expected that the DCFs outperform the nDCFs. Indeed, this is true for six of the seven functional pairs considered. XDM6, B97-D, LC-VV10, B2PLYP-D, XDM10, and ωB97X-D outperform their parent functionals by factors of 8.64, 6.78, 6.56, 3.00, 2.35, and 1.94, respectively, with respect to the total RMSD of the binding energies. The three that certainly stand out are XDM6, B97-D, and LC-VV10, since the addition of their respective dispersion correction improves the total RMSD of the parent functional by more than a factor of 6. The performance of XDM6 is noteworthy in particular, as it ranks sixth overall (behind XYGJ-OS, XYG3, ωB97X-2, MP2, and M11) for the total RMSD of the binding energies. The additional parameter of XDM10 seems to act as a disadvantage relative to XDM6, as XDM10 performs more than 3 times worse than its single-parameter relative for the binding energies. While the improvement of B2PLYP-D over B2PLYP is considerable, the addition of the dispersion tail transforms the parent functional's drastic underbinding (MSE of 2.28 kcal/mol) into moderate overbinding (MSE of −0.69 kcal/mol). On the contrary, the 2-fold improvement of ωB97X-D over ωB97X results only from reducing the overbinding of the parent functional, while maintaining the sign of the MSE.

The dramatic improvements that result from adding the XDM6, -D2, and VV10 corrections to B3LYP, B97, and LC-ωPBE are beautifully portrayed in Figure 2. By simply adding the dispersion correction, the drastic underbinding of the parent functional that deteriorates as the number of water molecules increases is replaced by mild underbinding or overbinding that is bound by a maximum MSE of 1 kcal/mol on either side. The performance of the VV10 NLC functional is interesting, as it improves the performance of LC-ωPBE for E_{bind} yet worsens the performance of rPW86. In both cases, the addition of the NLC functional results in a switch from underbinding to overbinding. However, for the case of rPW86, this leads to massive overbinding, while for LC-ωPBE, it leads to only slight overbinding. In Figure 6, an interesting phenomenon can be noticed when comparing the binding energy errors of the DCFs and the corresponding nDCFs. For all of the nDCFs except ωB97X, the addition of the dispersion correction leads to greater binding as expected. However, for ωB97X, the addition of the dispersion tail actually leads to less binding. This can be explained by remembering that the dispersion correction of ωB97X-D was retrained along with all of the empirical parameters of the functional.

4. DISCUSSION

In this section, the main results from the preceding analysis will be discussed with the help of Tables 4 and 5.

Table 4 ranks all 26 methods according to their performance for the relative and binding energies. With respect to the relative energy, the nine best methods are MP2, XYG3, B2PLYP, ωB97X-2, M11, B97, LC-ωPBE, XYGJ-OS, and M11-L, all with total E_{rel} RMSDs under 0.30 kcal/mol. All of these methods, except M11-L, contain an exact exchange component, with the top three having 100%, 80%, and 53%, respectively. In the binding energy category, the five best methods are XYGJ-OS, XYG3, ωB97X-2, MP2, and M11, all with total E_{bind} RMSDs under 0.4 kcal/mol. Of these five, the first four incorporate a fraction of MP2 correlation energy into their total energy, while the latter is a range-separated hybrid meta-GGA functional. The values for the BAR are informative because they help identify methods whose binding energy errors are highly

Table 4. Methods Ranked with Respect to Total Relative and Binding Energy RMSDs[a]

	E_{rel}		E_{bind}
MP2/a(TQ)Z	0.10	XYGJ-OS/aTZ	0.26
XYG3/aTZ	0.19	XYG3/aTZ	0.31
B2PLYP/a(TQ)Z	0.21	ωB97X-2/a(TQ)Z	0.31
ωB97X-2/a(TQ)Z	0.22	MP2/a(TQ)Z	0.34
M11	0.23	M11	0.38
B97	0.24	XDM6	0.52
LC-ωPBE	0.25	LC-VV10	0.62
XYGJ-OS/aTZ	0.28	M06	0.71
M11-L	0.29	B97-D	0.76
B3LYP	0.33	ωB97X-D	0.79
M06-2X	0.35	B2PLYP-D/a(TQ)Z	0.89
LC-VV10	0.37	M06-2X	1.02
XDM10	0.43	ωB97X	1.54
TPSSh	0.45	PBE	1.73
ωB97X	0.51	XDM10	1.93
XDM6	0.58	rPW86	2.08
TPSS	0.59	B2PLYP/a(TQ)Z	2.68
M06	0.62	M11-L	2.69
B2PLYP-D/a(TQ)Z	0.68	VV10	3.35
rPW86	0.79	LC-ωPBE	4.07
B97-D	0.79	TPSSh	4.20
PBE	0.95	TPSS	4.30
ωB97X-D	0.99	B3LYP	4.53
VV10	1.34	B97	5.15
HF	2.32	HF	11.48
SVWN	3.71	SVWN	14.21

[a]Results for the double hybrid density functionals are presented in the basis that most closely resembles the basis in which the respective functionals were parametrized (aug-cc-pV(TQ)Z for ωB97X-2, B2PLYP, and B2PLYP-D and aug-cc-pVTZ for XYG3 and XYGJ-OS). The MP2 results are from aug-cc-pV(TQ)Z calculations, while the results for the remaining functionals are presented in the aug-cc-pVQZ basis set.

Table 5. Dispersion-Corrected Functionals Ranked with Respect to Two Criteria[a]

DCF:nDCF	E_{rel}	nDCF:DCF	E_{bind}
XDM10:B3LYP	1.29	B3LYP:XDM6	8.64
LC-VV10:LC-ωPBE	1.46	B97:B97-D	6.78
VV10:rPW86	1.69	LC-ωPBE:LC-VV10	6.56
XDM6:B3LYP	1.74	B2PLYP:B2PLYP-D	3.00
ωB97X-D:ωB97X	1.95	B3LYP:XDM10	2.35
B2PLYP-D:B2PLYP	3.24	ωB97X:ωB97X-D	1.94
B97-D:B97	3.24	rPW86:VV10	0.62

[a]The first column contains the DCF:nDCF ratio of the total relative energy RMSD, while the second column contains the nDCF:DCF ratio of the total binding energy RMSD. All of the results (except B2PLYP-D and B2PLYP) are from calculations in the aug-cc-pVQZ basis set. The B2PLYP-D and B2PLYP results are from aug-cc-pV(TQ)Z calculations.

systematic. The four density functionals with the largest BAR are B97, LC-ωPBE, B3LYP, and B2PLYP, all with BARs larger than 15. These functionals suffer only in the binding energy category and perform competitively for the relative energies. Thus, dispersion-corrected versions of these functionals were assessed in order to determine if dispersion correction functionals can capture the missing information without altering the performance of the parent functional for the relative energies.

Before commenting further on dispersion-corrected functionals, it is helpful to revisit Figure 2 and realize that the mean signed error of the binding energy increases linearly with respect to the number of water molecules for all of the density functionals that perform poorly. Therefore, it is worthwhile to analyze the change in the MSE with respect to the number of water molecules in order to develop an "alignment correction" that can account for systematic underbinding and overbinding errors and make these functionals useful for application to larger clusters. For this analysis, B97 was chosen because it displayed the most severe and systematic underbinding of all of the methods considered. Performing a linear fit to the $n = 3-5$ binding energy mean signed errors of B97 resulted in a line with the equation: $y = 2.21x - 6.62$. Using this equation, the correction to the $n = 6$ binding energies was calculated to be 6.64 kcal/mol. By simply subtracting 6.64 kcal/mol from the $n = 6$ binding energies of B97, the $n = 6$ RMSD of B97 changed from 7.21 to 0.59 kcal/mol. Since this method applies a constant energy lowering to the binding energies, it is most effective for functionals that have a small total E_{rel} RMSD, since that is a measure of the parallelity of the binding energies to the reference binding energies. Thus, B97 is the perfect candidate for a fix of this kind. Using the same equation, the $n = 3-5$ binding energies were fixed by subtracting 0.01, 2.22, and 4.43 kcal/mol, respectively, from the binding energies of B97. The "corrected" B97 functional has a total binding energy RMSD of only 0.50 kcal/mol, more than 10 times smaller than its original RMSD of 5.15 kcal/mol. Thus, it is clear that a post-SCF analysis of this kind can be useful when considering sulfate−water clusters with larger numbers of water molecules.

The effect of dispersion correction functionals was explored in section 3.3, and the results are summarized in Table 5. To recap, the performance of the DCFs will be assessed by considering two criteria: the extent to which they *preserve* the performance of their parent functional for the relative energies (column 1 of Table 5) and the extent to which they *improve* the performance of their parent functional for the binding energies (column 2 of Table 5). The dispersion correction functional that best preserves the performance of its parent functional for the relative energies is XDM10. Conversely, the addition of the -D2 correction to B2PLYP and B97 has the most detrimental effect on the parent functional, increasing the total E_{rel} RMSD by a factor of 3.24 in both cases. While XDM10 does a good job of preserving the performance of B3LYP for the relative energies, it corrects the drastic underbinding of B3LYP by only a factor of 2.35, while XDM6 enhances the performance of B3LYP by a factor of 8.64. The -D2 correction to B97 manages to reduce the underbinding of B97 by a factor of 6.78, and appending VV10 to LC-ωPBE improves its performance for the binding energies by a factor of 6.56. Ultimately, LC-VV10 and XDM6 preserve the performance of their parent functionals (LC-ωPBE and B3LYP) for the relative energies almost as well as XDM10. Therefore, of the seven DCFs, LC-VV10 and XDM6 are the most successful.

5. CONCLUSIONS

As the search for the exact density functional continues, benchmarks that identify shortcomings in density functionals help developers make further improvements and refinements to existing models. In the preceding analysis and discussion, the performance of 24 density functionals, Hartree−Fock, and MP2

has been evaluated on a very specific chemical problem: sulfate−water clusters. The main conclusions from the benchmark, including the recommended methods for similar applications, are listed below:

- From the 26 benchmarked methods, MP2 has the best overall performance with respect to the CCSD(T)/CBS* reference values. Its total relative energy RMSD of only 0.10 kcal/mol is two times smaller than the best double hybrid density functional, and its total binding energy RMSD of 0.34 kcal/mol is only 0.08 kcal/mol larger than that of the best benchmarked method.
- After MP2, the three double hybrid density functionals (XYG3, ωB97X-2, and XYGJ-OS) have the best overall performance. These functionals perform slightly better than MP2 in the binding energy category but have a total relative energy RMSD that is at least twice the magnitude of the MP2 total relative energy RMSD. Furthermore, it is vital that these double hybrid density functionals be employed in a basis that is similar to the basis in which they were parametrized.
- M11 is the best density functional among the GGA, meta-GGA, hybrid GGA, hybrid meta-GGA, and dispersion-corrected density functionals.
- The best dispersion-corrected density functional is LC-VV10. While dispersion correction functionals can drastically improve the underbinding of their parent functionals for the binding energies of the sulfate−water clusters, it is equally important for them to maintain the quality of the parent functionals for the relative energies. Unfortunately, all of the dispersion correction functionals considered in this paper worsen the performance of their parent functional with respect to the relative energies. Even though LC-VV10 is the recommended dispersion-corrected functional, it is not competitive with MP2, XYG3, ωB97X-2, XYGJ-OS, and M11.
- Exact exchange is vital for predicting accurate relative energies. The best density functional that does not include any exact exchange is M11-L. However, M11-L performs surprisingly well for the relative energies but systematically underbinds the isomers. Fortunately, systematic errors in the binding energies can be easily fixed by an "alignment correction," as was shown with B97.

From the results presented in this paper, it is clear that the key to performing well in both categories considered is a balanced treatment of exchange and correlation. Ultimately, the five best methods are MP2, XYG3, ωB97X-2, XYGJ-OS, and M11.

■ ASSOCIATED CONTENT

Supporting Information

The updated CCSD(T)/CBS* relative and binding energies for the 49 sulfate−water clusters are included. Furthermore, relative and binding energy RMSDs as well as binding energy MSEs in the aug-cc-pVTZ, aug-cc-pVQZ, and (when applicable) aug-cc-pV(TQ)Z basis sets for all benchmarked methods are included. This information is available free of charge via the Internet at http://pubs.acs.org/.

■ AUTHOR INFORMATION

Corresponding Author

*E-mail: mhg@cchem.berkeley.edu.

Notes

The authors declare no competing financial interest.

■ ACKNOWLEDGMENTS

This work was supported in part by the U.S. Department of Energy under Contract No. DE-AC02-05CH11231, and by supercomputing resources provided by NERSC. A portion of the computations were performed at EMSL, a national scientific user facility sponsored by DOE's Office of Biological and Environmental Research and located at PNNL. This work was supported in part by the US Department of Energy, Office of Basic Energy Sciences, Division of Chemical Sciences, Geosciences & Biosciences (S.S.X.). Pacific Northwest National Laboratory (PNNL) is a multiprogram national laboratory operated for DOE by Battelle. We thank Teresa Head-Gordon for providing computational resources. We also acknowledge computational resources obtained under NSF award CHE-1048789.

■ REFERENCES

(1) Hohenberg, P.; Kohn, W. *Phys. Rev.* **1964**, *136*, B864−B871.
(2) Kohn, W.; Sham, L. J. *Phys. Rev.* **1965**, *140*, A1133−A1138.
(3) Perdew, J. P.; Ruzsinszky, A.; Tao, J.; Staroverov, V. N.; Scuseria, G. E.; Csonka, G. I. *J. Chem. Phys.* **2005**, *123*, 062201.
(4) Goerigk, L.; Grimme, S. *J. Chem. Theory Comput.* **2011**, *7*, 291−309.
(5) Goerigk, L.; Grimme, S. *Phys. Chem. Chem. Phys.* **2011**, *13*, 6670−6688.
(6) Burns, L. A.; Vázquez-Mayagoitia, A.; Sumpter, B. G.; Sherrill, C. D. *J. Chem. Phys.* **2011**, *134*, 084107.
(7) Chan, B.; Gill, P. M. W.; Radom, L. *J. Chem. Theory Comput.* **2012**, *8*, 4899−4906.
(8) Vydrov, O. A.; Van Voorhis, T. *J. Chem. Theory Comput.* **2012**, *8*, 1929−1934.
(9) Marom, N.; Tkatchenko, A.; Rossi, M.; Gobre, V. V.; Hod, O.; Scheffler, M.; Kronik, L. *J. Chem. Theory Comput.* **2011**, *7*, 3944−3951.
(10) Korth, M.; Thiel, W. *J. Chem. Theory Comput.* **2011**, *7*, 2929−2936.
(11) Mardirossian, N.; Parkhill, J. A.; Head-Gordon, M. *Phys. Chem. Chem. Phys.* **2011**, *13*, 19325−19337.
(12) Bergström, P.-A.; Lindgren, J.; Kristiansson, O. *J. Phys. Chem.* **1991**, *95*, 8575−8580.
(13) Cannon, W. R.; Pettitt, B. M.; McCammon, J. A. *J. Phys. Chem.* **1994**, *98*, 6225−6230.
(14) Jungwirth, P.; Curtis, J. E.; Tobias, D. J. *Chem. Phys. Lett.* **2003**, *367*, 704−710.
(15) Wang, X.-B.; Yang, X.; Nicholas, J. B.; Wang, L.-S. *Science (Washington, DC, U. S.)* **2001**, *294*, 1322−1325.
(16) O'Brien, J. T.; Prell, J. S.; Bush, M. F.; Williams, E. R. *J. Am. Chem. Soc.* **2010**, *132*, 8248−8249.
(17) Yang, X.; Wang, X.-B.; Wang, L.-S. *J. Phys. Chem. A* **2002**, *106*, 7607−7616.
(18) Zhou, J.; Santambrogio, G.; Brümmer, M.; Moore, D. T.; Wöste, L.; Meijer, G.; Neumark, D. M.; Asmis, K. R. *J. Chem. Phys.* **2006**, *125*, 111102.
(19) Bush, M. F.; Saykally, R. J.; Williams, E. R. *J. Am. Chem. Soc.* **2007**, *129*, 2220−2221.
(20) Wang, X.-B.; Sergeeva, A. P.; Yang, J.; Xing, X.-P.; Boldyrev, A. I.; Wang, L.-S. *J. Phys. Chem. A* **2009**, *113*, 5567−5576.
(21) Lambrecht, D. S.; McCaslin, L.; Xantheas, S. S.; Epifanovsky, E.; Head-Gordon, M. *Mol. Phys.* **2012**, *0*, 1−9.
(22) Perdew, J. P.; Burke, K.; Ernzerhof, M. *Phys. Rev. Lett.* **1996**, *77*, 3865−3868.

(23) Murray, E. D.; Lee, K.; Langreth, D. C. *J. Chem. Theory Comput.* **2009**, *5*, 2754−2762.
(24) Tao, J.; Perdew, J. P.; Staroverov, V. N.; Scuseria, G. E. *Phys. Rev. Lett.* **2003**, *91*, 146401.
(25) Peverati, R.; Truhlar, D. G. *J. Phys. Chem. Lett.* **2012**, *3*, 117−124.
(26) Becke, A. D. *J. Chem. Phys.* **1993**, *98*, 5648−5652.
(27) Becke, A. D. *J. Chem. Phys.* **1997**, *107*, 8554−8560.
(28) Chai, J.-D.; Head-Gordon, M. *J. Chem. Phys.* **2008**, *128*, 084106.
(29) Vydrov, O. A.; Scuseria, G. E. *J. Chem. Phys.* **2006**, *125*, 234109.
(30) Staroverov, V. N.; Scuseria, G. E.; Tao, J.; Perdew, J. P. *J. Chem. Phys.* **2003**, *119*, 12129−12137.
(31) Zhao, Y.; Truhlar, D. *Theor. Chem. Acc.* **2008**, *120*, 215−241.
(32) Peverati, R.; Truhlar, D. G. *J. Phys. Chem. Lett.* **2011**, *2*, 2810−2817.
(33) Chai, J.-D.; Head-Gordon, M. *J. Chem. Phys.* **2009**, *131*, 174105.
(34) Grimme, S. *J. Chem. Phys.* **2006**, *124*, 034108.
(35) Zhang, Y.; Xu, X.; Goddard, W. A. *Proc. Natl. Acad. Sci. U. S. A.* **2009**, *106*, 4963−4968.
(36) Zhang, I. Y.; Xu, X.; Jung, Y.; Goddard, W. A. *Proc. Natl. Acad. Sci. U. S. A.* **2011**, *108*, 19896−19900.
(37) Vydrov, O. A.; Voorhis, T. V. *J. Chem. Phys.* **2010**, *133*, 244103.
(38) Becke, A. D.; Johnson, E. R. *J. Chem. Phys.* **2005**, *123*, 154101.
(39) Becke, A. D.; Johnson, E. R. *J. Chem. Phys.* **2005**, *122*, 154104.
(40) Johnson, E. R.; Becke, A. D. *J. Chem. Phys.* **2005**, *123*, 024101.
(41) Becke, A. D.; Johnson, E. R. *J. Chem. Phys.* **2006**, *124*, 014104.
(42) Johnson, E. R.; Becke, A. D. *J. Chem. Phys.* **2006**, *124*, 174104.
(43) Kong, J.; Gan, Z.; Proynov, E.; Freindorf, M.; Furlani, T. R. *Phys. Rev. A* **2009**, *79*, 042510.
(44) Grimme, S. *J. Comput. Chem.* **2006**, *27*, 1787−1799.
(45) Chai, J.-D.; Head-Gordon, M. *Phys. Chem. Chem. Phys.* **2008**, *10*, 6615−6620.
(46) Schwabe, T.; Grimme, S. *Phys. Chem. Chem. Phys.* **2007**, *9*, 3397−3406.
(47) Pérez-Jordá, J. M.; Becke, A. D. *Chem. Phys. Lett.* **1995**, *233*, 134−137.
(48) Kristyán, S.; Pulay, P. *Chem. Phys. Lett.* **1994**, *229*, 175−180.
(49) Hobza, P.; Šponer, J.; Reschel, T. *J. Comput. Chem.* **1995**, *16*, 1315−1325.
(50) Patton, D. C.; Pederson, M. R. *Phys. Rev. A* **1997**, *56*, R2495−R2498.
(51) Milet, A.; Korona, T.; Moszynski, R.; Kochanski, E. *J. Chem. Phys.* **1999**, *111*, 7727−7735.
(52) Ruzsinszky, A.; Perdew, J. P.; Csonka, G. I.; Vydrov, O. A.; Scuseria, G. E. *J. Chem. Phys.* **2007**, *126*, 104102.
(53) Ruzsinszky, A.; Perdew, J. P.; Csonka, G. I.; Vydrov, O. A.; Scuseria, G. E. *J. Chem. Phys.* **2006**, *125*, 194112.
(54) Elstner, M.; Hobza, P.; Frauenheim, T.; Suhai, S.; Kaxiras, E. *J. Chem. Phys.* **2001**, *114*, 5149−5155.
(55) Wu, X.; Vargas, M. C.; Nayak, S.; Lotrich, V.; Scoles, G. *J. Chem. Phys.* **2001**, *115*, 8748−8757.
(56) Wu, Q.; Yang, W. *J. Chem. Phys.* **2002**, *116*, 515−524.
(57) Grimme, S. *J. Comput. Chem.* **2004**, *25*, 1463−1473.
(58) Jurečka, P.; Černy, J.; Hobza, P.; Salahub, D. R. *J. Comput. Chem.* **2007**, *28*, 555−569.
(59) Grimme, S.; Antony, J.; Ehrlich, S.; Krieg, H. *J. Chem. Phys.* **2010**, *132*, 154104.
(60) Rohrdanz, M. A.; Martins, K. M.; Herbert, J. M. *J. Chem. Phys.* **2009**, *130*, 054112.
(61) Henderson, T. M.; Janesko, B. G.; Scuseria, G. E. *J. Chem. Phys.* **2008**, *128*, 194105.
(62) Song, J.-W.; Hirosawa, T.; Tsuneda, T.; Hirao, K. *J. Chem. Phys.* **2007**, *126*, 154105.
(63) Baer, R.; Neuhauser, D. *Phys. Rev. Lett.* **2005**, *94*, 043002.
(64) Livshits, E.; Baer, R. *Phys. Chem. Chem. Phys.* **2007**, *9*, 2932−2941.
(65) Heyd, J.; Scuseria, G. E. *J. Chem. Phys.* **2004**, *120*, 7274−7280.
(66) Adamson, R. D.; Dombroski, J. P.; Gill, P. M. W. *J. Comput. Chem.* **1999**, *20*, 921−927.
(67) Leininger, T.; Stoll, H.; Werner, H.-J.; Savin, A. *Chem. Phys. Lett.* **1997**, *275*, 151−160.
(68) Gill, P. M. W.; Adamson, R. D.; Pople, J. A. *Mol. Phys.* **1996**, *88*, 1005−1009.
(69) Gerber, I. C.; Ángyán, J. *Chem. Phys. Lett.* **2005**, *415*, 100−105.
(70) Iikura, H.; Tsuneda, T.; Yanai, T.; Hirao, K. *J. Chem. Phys.* **2001**, *115*, 3540−3544.
(71) Heyd, J.; Scuseria, G. E.; Ernzerhof, M. *J. Chem. Phys.* **2003**, *118*, 8207−8215.
(72) Tawada, Y.; Tsuneda, T.; Yanagisawa, S.; Yanai, T.; Hirao, K. *J. Chem. Phys.* **2004**, *120*, 8425−8433.
(73) Lambrecht, D. S.; Clark, G. N. I.; Head-Gordon, T.; Head-Gordon, M. *J. Phys. Chem. A* **2011**, *115*, 11438−11454.
(74) Wang, X.-B.; Nicholas, J. B.; Wang, L.-S. *J. Chem. Phys.* **2000**, *113*, 10837−10840.
(75) Blades, A. T.; Kebarle, P. *J. Am. Chem. Soc.* **1994**, *116*, 10761−10766.
(76) Wang, X.-B.; Nicholas, J. B.; Wang, L.-S. *J. Chem. Phys.* **2000**, *113*, 653−661.
(77) Ponder, J. W.; Wu, C.; Ren, P.; Pande, V. S.; Chodera, J. D.; Schnieders, M. J.; Haque, I.; Mobley, D. L.; Lambrecht, D. S.; DiStasio, R. A.; Head-Gordon, M.; Clark, G. N. I.; Johnson, M. E.; Head-Gordon, T. *J. Phys. Chem. B* **2010**, *114*, 2549−2564.
(78) Wolinski, K.; Pulay, P. *J. Chem. Phys.* **2003**, *118*, 9497−9503.
(79) Jurgens-Lutovsky, R.; Almlöf, J. *Chem. Phys. Lett.* **1991**, *178*, 451−454.
(80) Liang, W.; Head-Gordon, M. *J. Phys. Chem. A* **2004**, *108*, 3206−3210.
(81) Steele, R. P.; DiStasio, R. A.; Shao, Y.; Kong, J.; Head-Gordon, M. *J. Chem. Phys.* **2006**, *125*, 074108.
(82) Distasio, R. A.; Steele, R. P.; Head-Gordon, M. *Mol. Phys.* **2007**, *105*, 2731−2742.
(83) Steele, R. P.; Head-Gordon, M. *Mol. Phys.* **2007**, *105*, 2455−2473.
(84) Steele, R. P.; Shao, Y.; DiStasio, R. A.; Head-Gordon, M. *J. Phys. Chem. A* **2006**, *110*, 13915−13922.
(85) Halkier, A.; Helgaker, T.; Jørgensen, P.; Klopper, W.; Koch, H.; Olsen, J.; Wilson, A. K. *Chem. Phys. Lett.* **1998**, *286*, 243−252.
(86) Shao, Y.; et al. *Phys. Chem. Chem. Phys.* **2006**, *8*, 3172−3191.
(87) Wheeler, S. E.; Houk, K. N. *J. Chem. Theory Comput.* **2010**, *6*, 395−404.
(88) Valiev, M.; Bylaska, E. J.; Govind, N.; Kowalski, K.; Straatsma, T. P.; Van Dam, H. J. J.; Wang, D.; Nieplocha, J.; Apra, E.; Windus, T. L.; de Jong, W. A. NWChem: A comprehensive and scalable open-source solution for large scale molecular simulations. *Comput. Phys. Commun.* **2010**, *181* (9), 1477−1489.